



# Spatial and spectral Quaternionic approaches for Colour Images

Patrice DENIS<sup>a,\*</sup>, Philippe CARRE<sup>a</sup>,  
Christine FERNANDEZ-MALOIGNE<sup>a</sup>

<sup>a</sup>University of Poitiers - SIC Laboratory - Bat SP2MI - Bd Marie et Pierre Curie  
B.P. 30179 - 86962 Futuroscope Chasseneuil Cedex - FRANCE

---

## Abstract

Hypercomplex or quaternions numbers have been used recently for both greyscale and colour image processing. Fast, numerous hypercomplex 2D Fourier transforms were presented as a generalization of the complex 2D Fourier transform to this new hypercomplex space. Thus, the major problem was to put an interpretation of what information the Fourier coefficients could provide. In this paper, we first define the conditions on the spectrum coefficients needed to reconstruct a colour image without loss of information through the inverse quaternionic Fourier transform process. The result is used to interpret the quaternionic spectrum coefficients of this specific colour Fourier transform. Secondly, with this apprehension of the quaternion numbers and the corresponding colour spectrum space, we define spatial and frequential strategies to filter colour images.

*Key words:* quaternions, quaternionic Fourier transform, colour image processing, filter, symmetry conditions

---

*NOTICE: this is the author's version of a work that was accepted for publication in Computer Vision and Image Understanding. Changes resulting from the publishing process, such as peer review, editing, corrections, structural formatting, and other quality control mechanisms may not be reflected in this document. Changes may have been made to this work since it was submitting for publication. A definitive version was subsequently published in Patrice DENIS, Philippe CARRE and Christine FERNANDEZ-MALOIGNE, Spatial*

---

\* Corresponding author.

*Email addresses:* [denis@sic.sp2mi.univ-poitiers.fr](mailto:denis@sic.sp2mi.univ-poitiers.fr) (Patrice DENIS),  
[carre@sic.sp2mi.univ-poitiers.fr](mailto:carre@sic.sp2mi.univ-poitiers.fr) (Philippe CARRE),  
[fernandez@sic.sp2mi.univ-poitiers.fr](mailto:fernandez@sic.sp2mi.univ-poitiers.fr) (Christine FERNANDEZ-MALOIGNE).

*Preprint submitted to Computer Vision and Image Understanding*

*and spectral Quaternionic approaches for Colour Images, Computer Vision and Image Understanding, In Press, Accepted Manuscript, Available online 8 February 2007, . (<http://www.sciencedirect.com/science/article/B6WCX-4N0X5Y6-1/2/ebc9f4fb65da13b0c696dd3857391dfb>)*

Nowadays, as multimedia devices and internet are becoming accessible to more and more people, image processing must take colour information into account because colour processing is needed everywhere for new technologies. Several approaches have been submitted to deal with colour images, one of the oldest is to process each channel of the colour image separately. Implementing such programs often creates colour shifts and artefacts, so different approaches should be used to produce visually pleasing colour images. A quite recent approach is to encode the three channel components on the three imaginary parts of a quaternion as proposed by S.T. Sangwine and T. Ell in [20,14,13]. Quaternions have been used for both greyscale images by Bülow [1] and colour ones by Sangwine et al. [20]. An introduction of quaternionic Fourier transforms has been made independently by both the teams above but in different definitions. In this paper, we study the Quaternionic Fourier spectrum in order to define precisely the properties of this new colour representation. In this way, we want to explain the colour information contained in the new domain that is to say how the different real and imaginary parts of the spectral quaternionic domain interact with the pure quaternion component chosen to encode colours in spatial domain. The other fundamental studied topic in the paper is the filtering aspect. Indeed, we review spatial colour filter approaches, introduce a new spatial gradient approach using quaternions, and validate a new quaternionic spectral colour filter.

The first section of this paper reminds what the quaternions are and how to use them to process colour information. Then we study how quaternions can be used to make  $\mathbb{R}^3$  transformations such as projections, rotations, etc. As an example, these transformations are used to switch from RGB to HSV colour spaces. The second section introduces the discrete quaternionic Fourier transform proposed by Sangwine and by Bülow, and we define the conditions on the quaternionic spectrum to enable manipulations into this frequency domain without losing information when going back to the spatial domain. This is also the subject of the second section which gives a new interpretation of the influence of Dirac initialization on the quaternionic Fourier space. The third section starts by surveying existing colour image filtering approaches based on quaternions. Then, we use the  $\mathbb{R}^3$  transformations defined in the first section and the analysis of the quaternionic frequency domain in the second section to propose the definitions of a new quaternionic vector gradient and a frequency quaternionic filter. Finally, the appendix gives more details with formulas and graphics to help understand the information included in the quaternionic colour spectrum.

# 1 Quaternions

## 1.1 Concept

A quaternion  $q \in \mathbb{H}$  ( $\mathbb{H}$  refers to Hamilton[8] who was first to discover these numbers) is a generalization of a complex number and is defined as  $q = q_r + q_i i + q_j j + q_k k$  where:

- $q_r, q_i, q_j$  and  $q_k$  are real numbers.
- $i, j$  and  $k$  are three new imaginary numbers, asserting:

$$i^2 = j^2 = k^2 = -1 \quad ij = -ji = k \quad jk = -kj = i \quad \text{and} \quad ki = -ik = j$$

With  $q = q_r + q_i i + q_j j + q_k k$  any quaternion:

- $\bar{q} = q_r - q_i i - q_j j - q_k k$  is  $q$ 's conjugate.
- $q$ 's modulus or norm is  $\sqrt{q_r^2 + q_i^2 + q_j^2 + q_k^2} = \sqrt{q\bar{q}}$  noted  $|q|$ .
- if  $q \neq 0$ , then  $q^{-1} = \frac{\bar{q}}{|q|^2}$  is  $q$ 's inverse.
- $\Re(q) = q_r$  is  $q$ 's real part. If  $\Re(q) = q$ , then  $q$  is real.
- $\Im(q) = ib + jc + kd$  is  $q$ 's imaginary part. If  $\Im(q) = q$ , then  $q$  is pure.
- $\mathbb{P} = \{q \in \mathbb{H} \mid q = \Im(q)\}$  is the Pure Quaternion set.
- $\mathbb{S} = \{q \in \mathbb{H} \mid |q| = 1\}$  is the Unitary Quaternion set.

Note that the quaternion product is anti-commutative.

Quaternions can be expressed using scalar part  $S(q)$  and vector part  $V(q)$ ,  $q = S(q) + V(q)$  with  $S(q) = q_r$  and  $V(q) = q_i i + q_j j + q_k k$ . Sangwine and Ell [20,14,13,21,22,4] were the first to use this vector part of quaternions to encode colour images. They took the three imaginary parts to code the r (red), g (green) and b (blue) colour components of an image. A colour image  $I$  with the spatial resolution of  $N \times M$  pixels is in this way represented by an  $N \times M$  matrix as follow:

$$q(s, t) = r(s, t)i + g(s, t)j + b(s, t)k$$

where  $s = 1, 2, \dots, N$  and  $t = 1, 2, \dots, M$  are the spatial coordinates of the pixel  $q$ .

## 1.2 $\mathbb{R}^3$ Transformations with Quaternions

As pure quaternions are used analogously to describe  $\mathbb{R}^3$  vectors, the classical  $\mathbb{R}^3$  transformations such as translations, reflections, projections, rejections and rotations can be defined with only additions and multiplications as explained by Sangwine in [22] (cf. Figure 1). With two pure quaternions  $(q_1, q_2) \in \mathbb{P}^2$ , the translation vector is supported by the quaternion  $q_{trans} = q_1 + q_2$ . If  $q \in \mathbb{P}$  and  $\mu \in \mathbb{S} \cap \mathbb{P}$  then  $q_{refl} = -\mu q \mu$  is the  $q$ 's reflection vector with  $\mu$  axis. If  $q \in \mathbb{P}$  and  $\mu \in \mathbb{S} \cap \mathbb{P}$  then  $q_{proj} = \frac{1}{2}(q - \mu q \mu)$  is the  $q$ 's projection vector on  $\mu$  axis. If  $q \in \mathbb{P}$  and  $\mu \in \mathbb{S} \cap \mathbb{P}$  then  $q_{rej} = \frac{1}{2}(q + \mu q \mu)$  is the  $q$ 's orthogonal projection vector on  $\mu$  axis's orthogonal plane or the  $q$ 's rejection of the  $\mu$  axis. And eventually if  $q \in \mathbb{P}$ ,  $\phi \in \mathbb{R}$  and  $\mu \in \mathbb{S} \cap \mathbb{P}$  then  $q_{rot} = e^{\mu \frac{\phi}{2}} q e^{-\mu \frac{\phi}{2}}$  is the  $q$ 's rotation vector around  $\mu$  axis with  $\phi$  angle.

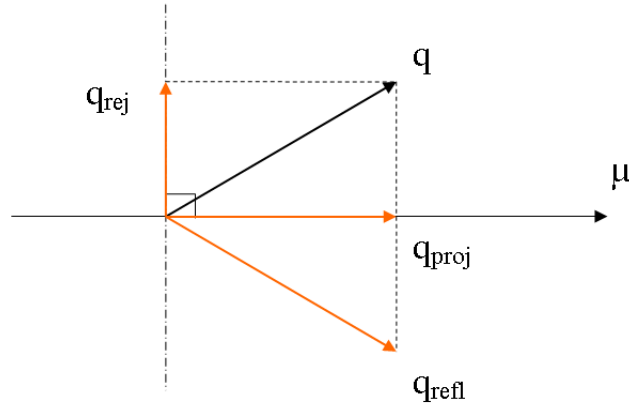


Fig. 1. **Geometric Transformations in  $\mathbb{R}^3$  with Quaternion:**  $q$  denotes the original vector,  $\mu$  denotes the axis vector,  $q_{refl}$  is the  $q$ 's reflection vector with  $\mu$  axis,  $q_{rej}$  is the  $q$ 's rejection of the  $\mu$  axis and  $q_{proj}$  is  $q$ 's projection vector on  $\mu$  axis.

For each colour pixel described in RGB colour space using a quaternion vector  $q \in \mathbb{P}$ , HSV (hue, saturation, value) colour space coordinates can be found using operations on quaternions. We consider that the value component of the HSV vector represents the norm of the colour's orthogonal projection vector  $(q \cdot \mu_{grey}) \mu_{grey}$  on the grey axis  $\mu_{grey}$  (this axis can be defined such that  $\mu_{grey} = \frac{i+j+k}{\sqrt{3}}$ ). Saturation and hue are represented on the plane orthogonal to the grey axis which crosses  $(q \cdot \mu_{grey}) \mu_{grey}$ . The saturation is the distance between the colour vector  $q$  and the grey axis  $\mu_{grey}$ , and hue is the angle between the colour vector  $q$  and a colour vector  $\nu$  taken anywhere on the plane orthogonal to  $\mu_{grey}$  and which sets the zero hue reference angle. This reference hue value is often taken to represent the red colour vector, so we decided arbitrarily to associate the red colour vector to the  $\nu$  vector and gave

it a zero hue value (cf. Figure 2). Hue is the angle between this reference colour vector and the colour vector  $q$ .

For a colour vector  $q$ , the corresponding H, V, and S components can be obtained using the grey-axis  $\mu = \mu_{grey} \in \mathbb{S} \cap \mathbb{P}$  and the reference colour vector  $\nu \in \mathbb{S} \cap \mathbb{P}$  with the following elementary quaternionic operations [7]

$$\begin{cases} H = \tan^{-1} \frac{|q - \mu\nu q \nu \mu|}{|q - \nu q \nu|} \\ S = \left| \frac{1}{2}(q + \mu q \mu) \right| \\ V = \left| \frac{1}{2}(q - \mu q \mu) \right| \end{cases} \quad (1)$$

which will be used later in this paper to define a new gradient operator.

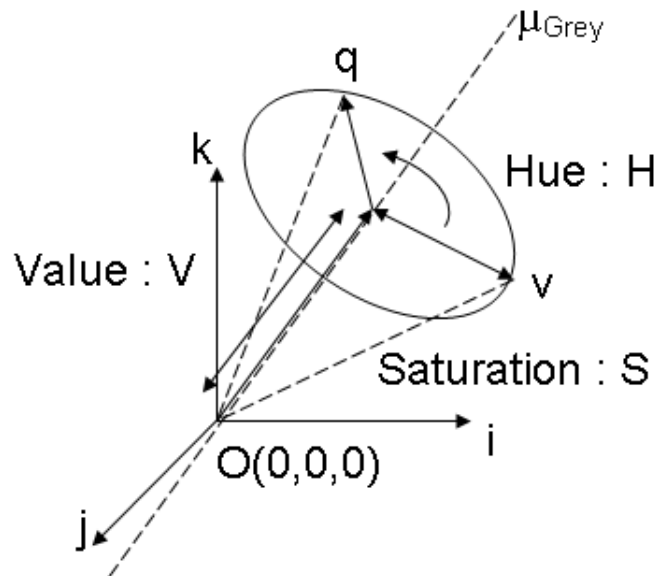


Fig. 2. Hue, Saturation and Value given with reference  $\mu_{Grey}$  and  $H(\nu) = 0$

## 2 Discrete Quaternion Fourier Transform

### 2.1 Definition

Different works introduced the quaternionic Fourier Transform, [1,21]. The Discrete Quaternion Fourier Transform (DQFT) in  $\mu = \mu_i i + \mu_j j + \mu_k k \in \mathbb{S} \cap \mathbb{P}$  direction analysis allows us to give the frequency equivalence of a  $N \times M$  spatial

colour image in a matrix defined by

$$Q(S, T) = \frac{1}{\sqrt{MN}} \sum_{s=-\frac{N}{2}+1}^{\frac{N}{2}} \sum_{t=-\frac{M}{2}+1}^{\frac{M}{2}} \exp^{-2\mu\pi(\frac{Ss}{N} + \frac{Tt}{M})} q(s, t) \quad (2)$$

Here, the term  $Q(S, T)$  represents the frequency coordinates and  $q(s, t) = r(s, t)i + g(s, t)j + b(s, t)k$  is a pure quaternion used to represent the three different colour channels of the pixel at the coordinates  $(s, t)$  of the colour image. Since the quaternion product is not commutative, DQFT can have different forms [15]. Note that in this paper we will follow the DQFT definition given in (2).

The inverse DQFT (IDQFT) to the transform presented in (2) is given by

$$q(s, t) = \frac{1}{\sqrt{MN}} \sum_{S=-\frac{N}{2}+1}^{\frac{N}{2}} \sum_{T=-\frac{M}{2}+1}^{\frac{M}{2}} \exp^{2\pi\mu(\frac{Ss}{N} + \frac{Tt}{M})} Q(S, T)$$

It is proved [15,5] that DQFT or its inverse (IDQFT) for a square matrix of dimension  $2^n \times 2^n$  could be simplified by processing two fast complex Fourier transforms.

## 2.2 Colour quaternion spectrum properties

In order to understand what the Fourier coefficients stand for, we studied the digital characterization of the DQFT. We first discovered that the colour Fourier spectrum exhibits some symmetries due to zero scalar spatial part of any colour image. This observation follows the well-known fact that the spectrum of a real signal by a complex Fourier transform (CFT) has hermitian properties of symmetry.

Even if the spatial information of a colour image is using pure quaternions only, applying a DQFT on an image results in full quaternions (i.e. with nonzero scalar part). We wanted to find, after IDQFT, a space where scalar part is zero in order to avoid any loss of information as the spatial colour image is coded on a pure quaternions matrix.

Let

$$Q(S, T) = Q_r(S, T) + Q_i(S, T)i + Q_j(S, T)j + Q_k(S, T)k$$

be the spectral quaternion at coordinates  $(S, T) \in ([-\frac{N}{2} + 1.. \frac{N}{2}], [-\frac{M}{2} + 1.. \frac{M}{2}])$ .

In addition, let

$$q(s, t) = q_i(s, t)i + q_j(s, t)j + q_k(s, t)k$$

denote the IDQFT quaternion of  $(s, t)$  spatial coordinates.

Developping this, with  $\mu = \mu_i i + \mu_j j + \mu_k k$ , the cartesian real part form of the spatial domain leads to

$$\begin{aligned} q_r(s, t) = & \frac{1}{\sqrt{MN}} \sum \sum \left[ \cos\left(2\pi \left(\frac{Ss}{N} + \frac{Tt}{M}\right)\right) Q_r(S, T) \right. \\ & - \mu_i \sin\left(2\pi \left(\frac{Ss}{N} + \frac{Tt}{M}\right)\right) Q_i(S, T) - \mu_j \sin\left(2\pi \left(\frac{Ss}{N} + \frac{Tt}{M}\right)\right) Q_j(S, T) \\ & \left. - \mu_k \sin\left(2\pi \left(\frac{Ss}{N} + \frac{Tt}{M}\right)\right) Q_k(S, T) \right] \end{aligned} \quad (3)$$

where  $q_r(s, t)$  is null when

$$\begin{aligned} Q_r(-S, -T) &= -Q_r(S, T) ; Q_i(-S, -T) = Q_i(S, T) \\ Q_j(-S, -T) &= Q_j(S, T) ; Q_k(-S, -T) = Q_k(S, T) \end{aligned}$$

As it can be seen from the symmetries contained in the Fourier spectrum, the real part must be odd and all the imaginary parts must be even. This is a direct extension of the antihermitian property of the complex Fourier transform of imaginary signal. Any transform in the quaternionic colour spectrum must obey to these rules to keep spatial information safe.

### 2.3 Digital study of the colour spectrum

In this section, we try to give an interpretation of the information contained in the quaternionic spectrum of colour images. To do this, we propose to initialize the discrete spectrum with a constant which will represent a Dirac (an infinitely short pulse) and study the response in the spatial domain after IDQFT. Note that the details of the calculus are presented in appendix.

Initialization could be done in two different ways:

- On the real part of the spectrum, this leads to odd oscillations on the spatial domain linked to the  $\mu$  direction parameter of the Fourier transform. Complex colours are obtained in the RGB colour space after modifying  $\mu$  and normalizing it in order to obtain a pure unit quaternion.

If  $Q_r(S_0, T_0) = K_r$ ;  $Q_r(-S_0, -T_0) = -K_r$  then

$$q(s, t) = 2K_r \left( \mu_i \sin\left(2\pi \left(\frac{S_0 s}{N} + \frac{T_0 t}{M}\right)\right) + \mu_j \sin\left(2\pi \left(\frac{S_0 s}{N} + \frac{T_0 t}{M}\right)\right) + \mu_k \sin\left(2\pi \left(\frac{S_0 s}{N} + \frac{T_0 t}{M}\right)\right) \right)$$

- On an imaginary part of the spectrum, this results to even oscillations on the spatial domain independently from the  $\mu$  parameter of the Fourier trans-

form. A proper initialization on the different imaginary components with respect to the additive colour synthesis theory allows to reach complex colours. For example to get yellow oscillations the red and green components (i and j) should be initialised (with  $e=i,j$  or  $k$ ).

$$\text{If } Q_e(S_0, T_0) = Q_e(-S_0, -T_0) = K_e \text{ then } q_e(s, t) = 2K_e\mu_e \cos\left(2\pi\left(\frac{S_0s}{N} + \frac{T_0t}{M}\right)\right)$$

#### 2.4 Quaternionic Graphical Spectrum Illustration

Figure 3 illustrates the different possible initializations on the quaternionic spectrum. A pair of constants has been set on the quaternionic spectrum following the properties for spatial reconstruction, then IDQFT has been performed to make the following subfigures (for more graphical illustrations report to section A.2 in the appendix).

- Initializing a pair of constants on any imaginary component with any direction  $\mu$  leads to a spatial oscillation on the same component (Figure 3(a)).
- Initializing a pair of constants on the real component leads to a spatial oscillation following the same imaginary component(s) as those included in the direction  $\mu$  (Figure 3(b)).
- The coordinates  $(S_0, T_0)$  and  $(-S_0, -T_0)$  of the two initialization points in the Fourier domain affect the orientation and the frequency of the oscillations in the spatial domain as it does so for greyscale image in complex Fourier domain. Orientation of the oscillations can be changed as shown in Figure 3(c).

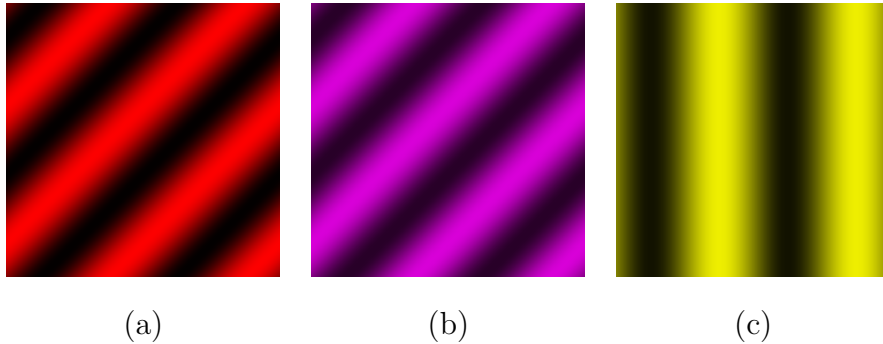


Fig. 3. **Spectrum Initialization examples:** (a)  $\mu_{Grey} = \frac{i+j+k}{\sqrt{3}}$  and  $Q_i(2, 2) = Q_i(-2, -2) = K_i$ ; (b)  $\mu_{Magenta} = \frac{i+k}{\sqrt{2}}$  and  $Q_r(2, 2) = -Q_r(-2, -2) = K_r$ ; (c)  $\mu_{Yellow} = \frac{i+j}{\sqrt{2}}$  and  $Q_r(0, 2) = -Q_r(0, -2) = K_r$

The following focuses on the use of quaternions in filtering which is one of the most frequently used low level image processing operations. We first review spatial colour image approaches and get a new spatial colour filter. Then starting from the interpretation of the quaternionic Fourier space that we made in this previous section, we introduce a quaternionic spectrum filter.

### 3 Quaternionic filtering

In this section, we focus on the colour filtering aspect and study discontinuity detection which is a fundamental issue of colour image processing such as edge detection and image analysis. A number of approaches can be used to detect the edges and fine details in colour images. The following briefly surveys well-known approaches.

#### 3.1 Spatial filtering

##### 3.1.1 Marginal methods

Marginal methods, adopted directly from greyscale image processing, process each channel of the colour image separately (Figure 4a). Thus, they are computationally simple and easy to implement. On the other hand, due to the omission of the essential spectral information during processing, many marginal methods have insufficient performance [11,12]. As presented in [10,11], edges can be detected in a component-wise manner or by applying the processing solution to the luminance signal. However, neither approach can detect the discontinuities in colour information.

##### 3.1.2 Vectorial methods

To avoid the drawbacks of marginal solutions, vectorial methods, such as those based on robust order statistics [12,16], process colour pixels as vectors (Figure 4b). In the design proposed by Di Zenzo [3], edges are detected using colour vectorial gradients. The vectorial methods usually have better performance compared to marginal solutions, however, the performance improvements are obtained at expense of the increased computational complexity.

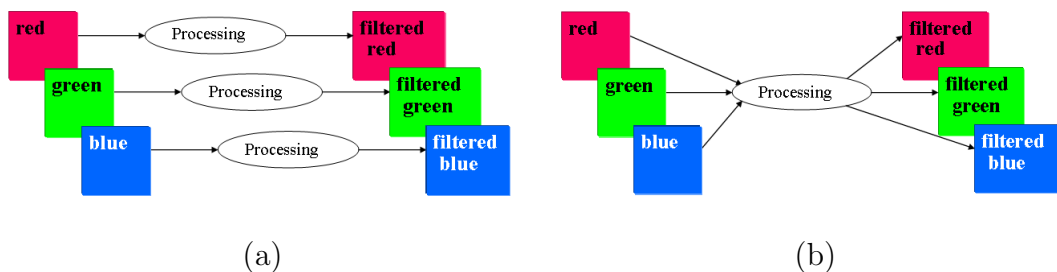


Fig. 4. (a) Marginal and (b) Vectorial methods

### 3.1.3 Perceptual methods

Perceptual methods [6,9,23,17] are based on the human visual system (HVS) characteristics. For example, in [2], Carron used a marginal gradient method but based on a weight factor : the hue coefficient of each pixel, more relevant than saturation or intensity to split colours. In a second approach, when the hue information is not enough to detect edges, the gradient is given using intensity and/or saturation. The contribution in this approach relies on the fact that if the difference between two colours is detected with a high saturation, the colours seem farther than if they have smaller saturation (i.e. nearer from the grey axis) but the same hues. Figure 5 shows that the two green vectors  $q_1$  and  $q_2$ , near the grey axis, seem to have a smaller hue difference than the two red vectors  $q_3$  and  $q_4$ , far from the grey axis. This is not true but there is a difference:  $q_1$  and  $q_2$  have a smaller saturation (distance from the grey axis) than  $q_3$  and  $q_4$ . The perceptual methods because using the HVS characteristics give better results than the marginal and vectorial ones. Moreover the chromatic information of pixels is used to avoid artefacts and a major advantage is the integration of colour shadows. Nevertheless, by working in proper colour spaces and using thresholds for instance for hue relevance, algorithms complexity is raised.

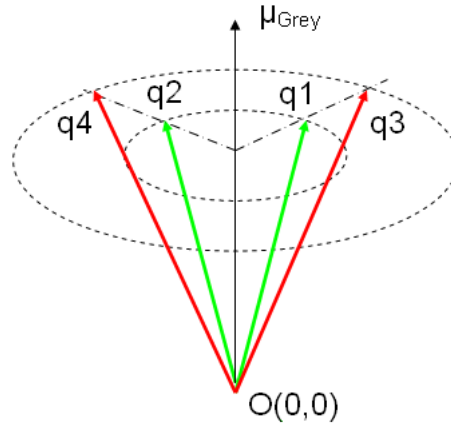


Fig. 5. The distance between  $q_1$  and  $q_2$  (green vectors) seems to be smaller than between  $q_3$  and  $q_4$  (red vectors) but the hue difference is the same:  $\widehat{q_1 q_2} = \widehat{q_3 q_4}$

### 3.1.4 Sangwine's quaternionic approach

Sangwine proposed the convolution on a quaternionic colour image can be defined by [20,14,21]:

$$q_{filtered}(s, t) = \sum_{\tau_1=-n_1}^{n_1} \sum_{\tau_2=-m_1}^{m_1} h_l(\tau_1, \tau_2) q((s - \tau_1)(t - \tau_2)) h_r(\tau_1, \tau_2) \quad (4)$$

where  $h_l$  and  $h_r$  are the two conjugate filters of dimension  $N_1 \times M_1$  where  $N_1 = 2n_1 + 1 \in \mathbb{N}$  and  $M_1 = 2m_1 + 1 \in \mathbb{N}$ .

From this definition of the convolution product, Sangwine proposed a colour edge detector in [19]. In this method, the two filters  $h_1$  and  $h_2$  are conjugated in order to fulfill a rotation operation of every pixel around the greyscale axis by an angle of  $\pi$  and compare it to its neighbours (cf. Figure 6).

$$q_{filt}(s, t) = l \star q \star r(s, t) \quad (5)$$

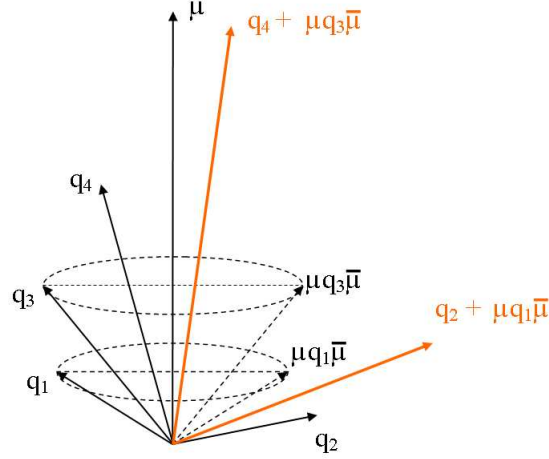


Fig. 6. **Sangwine's Edge Detector Scheme:**  $\mu$  is the grey axis;  $\mu q_1 \bar{\mu}$  (resp.  $\mu q_3 \bar{\mu}$ ) is the rotated vector of  $q_1$  (resp.  $q_3$ ) around  $\mu$  with an angle of  $\pi$ ; the comparison vector between  $q_1$  and  $q_2$  (resp. between  $q_3$  and  $q_4$ ) is given by  $q_2 + \mu q_1 \bar{\mu}$  (resp.  $q_4 + \mu q_3 \bar{\mu}$ );  $q_4 + \mu q_3 \bar{\mu}$  is near from the grey axis so the colour seems grey but  $q_2 + \mu q_1 \bar{\mu}$  is far from the grey axis so Sangwine's filter has detect an edge as this vector is more coloured.

The filter composed by a pair of quaternion conjugated filters is defined as follows

$$l = \frac{1}{6} \begin{bmatrix} 1 & 1 & 1 \\ 0 & 0 & 0 \\ Q & Q & Q \end{bmatrix} \quad \text{and} \quad r = \frac{1}{6} \begin{bmatrix} 1 & 1 & 1 \\ 0 & 0 & 0 \\ \bar{Q} & \bar{Q} & \bar{Q} \end{bmatrix} \quad (6)$$

where  $Q = e^{\mu \frac{\pi}{2}}$  and  $\mu = \mu_{Grey} = \frac{i+j+k}{\sqrt{3}}$  the greyscale axis.

The filtered image (cf. Figure 6) is a greyscale image almost everywhere, because in homogeneous regions the vector sum of one pixel to its neighbours rotated by  $\pi$  around the grey axis has a low saturation (cf.  $q_4 + \mu q_3 \bar{\mu}$  for instance). However, pixels in colour opposition (like  $q_1$  and  $q_2$  for example)

represent a colour edge. Therefore, they present a vector sum far from the grey axis. Edges are thus coloured due to this high distance.

Although this detector has a good performance, it often produces false colours, for example, when the vector sum is out of the colour space domain. Figure 7 shows that the edge of the hat is not detected by the same colour in c or d where the horizontal filtering convolution is applied rightwise or leftwise.



Fig. 7. **Sangwine edge detector result:** (a) original image; (b) Sangwine's filter applied from left to right horizontally; (c) zoom on the hat edge of the (b) picture; (d) same zoom but with the filter applied from right to left. Thus applying the filter leftwise in one same direction (horizontal, vertical or diagonal) leads to different results than applying it rightwise.

### 3.1.5 A new gradient detector

Starting with the result of Sangwine filter, we get for each pixel  $q_1$  and  $q_3$  a vector of itself rotated by  $\pi$  around the greyscale axis and compared to its neighbours  $q_2$  and  $q_4$ . We saw that the more the colour vector of a pixel is far from its neighbours (colour edge), the more the vector sum in Sangwine's

filter is far from the grey axis. Our approach also gives us a colour gradient. We propose to determine the distance  $q_{dist}$  of Sangwine's comparison colour vector sum  $q_{sum} = q_2 + \mu q_1 \bar{\mu}$  or  $q_{sum} = q_4 + \mu q_3 \bar{\mu}$  from the grey axis  $\mu$  (cf. Figure 8). This distance can be calculated with quaternionic operations (refer to section 1.2) and is the norm of the rejection of the vector of the grey axis. This distance is defined from a colour vector to the grey axis and we work in the RGB colour space. Thus, equation (1) implies that this is the saturation of the colour vector sum given by Sangwine's filter.

$$q_{dist} = \frac{1}{2}(q_{sum} + \mu q_{sum} \mu) \quad (7)$$

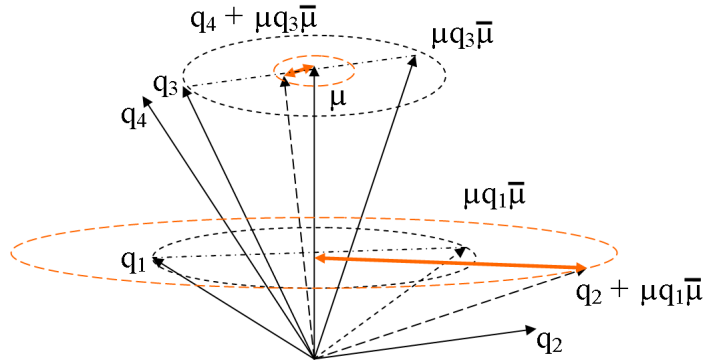


Fig. 8. **Proposed quaternionic edge detector:**  $\mu$  is the grey axis;  $\mu q_1 \bar{\mu}$  (resp.  $\mu q_3 \bar{\mu}$ ) is the rotated vector of  $q_1$  (resp.  $q_3$ ) around  $\mu$  with an angle of  $\pi$ ; our comparison vector between  $q_1$  and  $q_2$  (resp. between  $q_3$  and  $q_4$ ) is given by the distance  $q_{dist} = \frac{1}{2}(q_{sum} + \mu q_{sum} \mu)$  of Sangwine's vector sum  $q_{sum} = q_2 + \mu q_1 \bar{\mu}$  (resp.  $q_{sum} = q_4 + \mu q_3 \bar{\mu}$ ) from the grey axis (orange arrows); An edge is detected by a high distance from the grey axis like the orange arrow between  $\mu$  and  $q_2 + \mu q_1 \bar{\mu}$ .

Figure 9 shows that the two distances  $S_1$  and  $S_2$  are equal. Sangwine's filter gives two different colour vectors  $q_1 + \mu q_2 \bar{\mu}$  and  $q_2 + \mu q_1 \bar{\mu}$  for the same two original colours  $q_1$  and  $q_2$  comparison. Note that our new method is thus independent from the path (leftwise or rightwise) applied to convolute the filter with the image whereas Sangwine's is not.

This saturation filter is applied to the horizontal, vertical and both diagonal directions. The maximum of these values of saturation at each pixel of the image is then selected to make the final colour gradient filter by maximum distance. Note that this quaternionic filtering operation is linear but the total process is not linear as the "maximum" operator interferes.

Figure 10 shows the results of our experiment where in each row there are first the original image, then the colour gradient and log colour gradient (in order to amplify the edges detected by the colour gradient) and finally the edge map images. This last image is a thresholding on the colour gradient

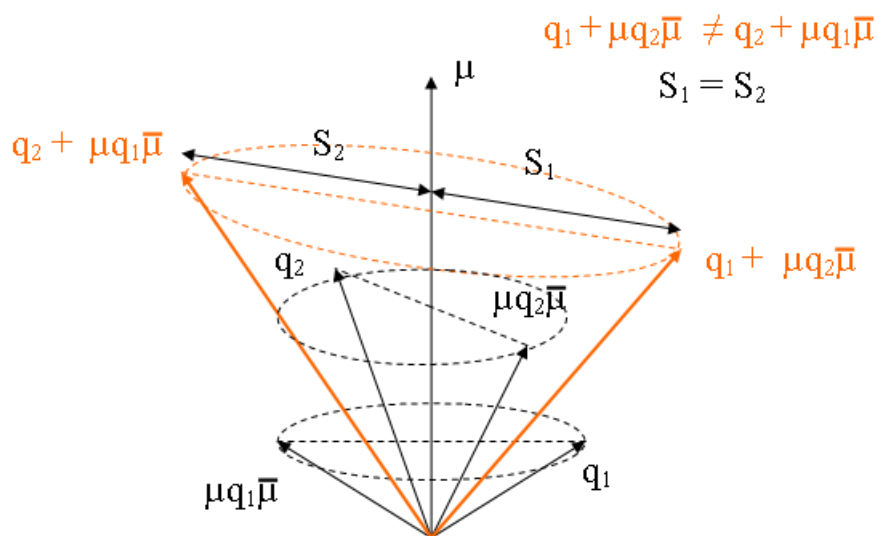


Fig. 9. **Difference between Sangwine and our edge detector:**  $\mu$  is the grey axis;  $\mu q_1 \bar{\mu}$  (resp.  $\mu q_2 \bar{\mu}$ ) is the rotated vector of  $q_1$  (resp.  $q_2$ ) around  $\mu$  with an angle of  $\pi$ ; the same colours  $q_1$  and  $q_2$  can give two different colour vectors  $q_{sum} = q_2 + \mu q_1 \bar{\mu}$  and  $q_{sum} = q_1 + \mu q_2 \bar{\mu}$  by the Sangwine's method. Note that our approach leads to the same distance because  $S_1 = S_2$ .

image. The results show that the method detect colour edges quite properly for example with the house image where walls, roof and sky are well separated. The same observation can be done with the well detected separation between Lenna's shoulder and chin. Process our method on images such as the mandrill separates correctly the homogeneous and textures areas. Even if there is still an edge detected between the roof and the top right side of the chimney, we can say that our approach handles shadows quite well. However, because our method uses a comparison of saturation only, the differences of luminance between colours is not detected, see for instance the details of the window's house.

### 3.1.6 Edge detection performance

Figure 11 shows the edge maps obtained using the different methods. The marginal (Figure 11b) and Di Zenzo (Figure 11c) approaches seem to be more sensitive to noise. The edges obtained by our approach (Figure 11f and g) are much thicker and closed. Remember that the first Carron method (Figure 11d) is based on a measure of the hue to weight the marginal gradient; the second method uses as well the saturation and the luminance measures to weight the gradient when hue is not enough relevant. These methods give closed contours and are not sensitive to noise as the marginal and Di Zenzo ones. Regarding Carron2 approach (Figure 11e), our method cannot distinguish as efficiently

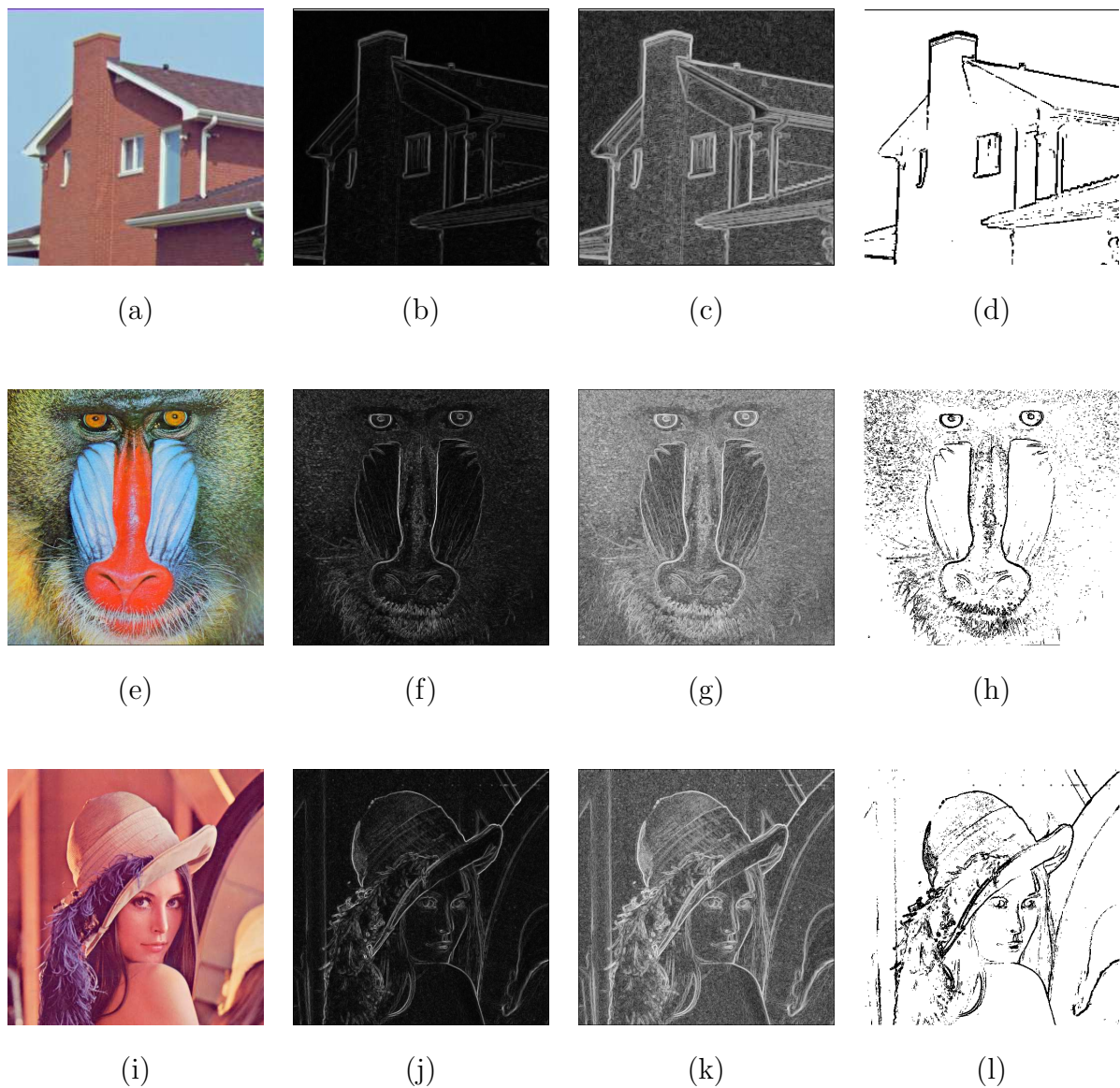


Fig. 10. From left to right, original images, colour gradient, log colour gradient and edge map from our new spatial method

shadows to real contours because our method is based on the saturation only. But this result depends on the thresholding done on the colour gradient. Indeed the shadows contours can be erased from our edge map but at the price of thinner edges everywhere else (see Figure 10d for example).

To improve our algorithm and take shadows into account we need to check if the saturation measure is self-sufficient. Indeed, two different colours can have the same saturation. It is the case for instance with  $q_1$  and  $q_2$  on one hand and  $q_3$  and  $q_4$  on the other hand as we saw in Figure 5. Even so,  $q_1$  and  $q_2$  are different colours as well as  $q_3$  and  $q_4$ , fortunately they can be disjoined by their difference of luminance and/or hue. Implementing these luminance and chromaticity measures (as the Carron2 method does) when saturation is not

enough relevant should enhance the performance of our approach.

Even with this lack of improvement, our edge detector is quite efficient with an implementation using quaternion formalism and the results are given without performing any change of colour space so imprecisions due to these digital manipulations of colours are avoided. Moreover, it should be noted that our edge detector is based on a vectorial approach and does not need any additional definition to sort colours. Our distance is a saturation one that does not give more importance for a specified colour than for another one, speaking at the same saturation level. Finally, our method is more similar to a perceptual one than those based on RGB colour space as it uses geometric concepts from HSV colour space for example.

### 3.1.7 Computational complexity

To compare the computational complexity of the proposed approach and the traditional marginal colour gradient operator, the quaternionic operations have to be expressed in terms of the traditional real operations such as multiplications and additions. Let  $mult_q$  (resp.  $mult_r$ ) stand for quaternionic (resp. real) multiplication,  $add_q$  (resp.  $add_r$ ) quaternionic (resp. real) addition:

- $add_q = 4 add_r$
- $mult_q = 4 * 4 mult_r + 4*3 add_r$

We apply Sangwine algorithm and then we calculate the distance of the colour sum vector results from the grey axis. Note that the calculations will be performed for a  $N \times N$  image.

- Sangwine algorithm :

Remember that for each pixel we apply two convolutions by a  $3 \times 3$  window, one with the quaternion  $Q$  and one with  $\overline{Q}$  (cf. equations (5) and (6)).

$$n_{Sang} = N^2(2 * (6mult_q + 5add_q))$$

In fact, since each convolution implies three zero coefficients, only 6 quaternionic multiplications and 5 quaternionic additions are needed.

- Distance calculation :

For each pixel again we calculate the saturation distance as seen in equation (7).

$$n_{Dist} = N^2(add_q + 2mult_q)$$

Then as we process the Sangwine filter on horizontal, vertical and both diagonal directions :

$$\begin{aligned}
n_{Total} &= 4 * (n_{Sang} + n_{Dist}) \\
&= 4 * (N^2(2 * (6 \text{ mult}_q + 5 \text{ add}_q)) + N^2(\text{add}_q + 2 \text{ mult}_q)) \\
&= N^2(832 \text{ mult}_r + 768 \text{ add}_r)
\end{aligned}$$

For a classical marginal gradient, the same kind of Prewitt filter is needed, but we only apply it one time on each colour component. We then apply it on the same four directions and the number of operations needed is about  $N^2(28\text{mult}_r + 20\text{add}_r)$ .

We can see that our method is using much more operations than the classical one so the computation time is increased (linearly and not exponentially). However, it should be noted that the complexity is not changed as both methods are in  $\mathcal{O}(N^2)$  and the results obtained using the proposed approach are better than the ones obtained using a marginal method.

### 3.2 Frequency filtering

Our approach is built on the same idea used to filter greyscale images: DQFT is performed on a colour image leading to its the frequential information. We then apply a mask on this Fourier information by setting its either low or high frequency coefficients to zero. Eventually, the result is processed through IDQFT to give the filtered image.

We use the quaternion formalism to encode colour images but we need to stay aware on the fact that the quaternionic product is not commutative. Indeed, the well known theorem which states that a convolution product in spatial domain is equal to the product in the Fourier space is not true with quaternions [15].

By definition, the formulation of our Fourier filtering approach is given by

$$q_{Filt} = IDQFT\{H.Q\} \tag{8}$$

with  $Q = DQFT(q)$  denotes the quaternionic Fourier transform of the original image and  $H$  the frequency behavior of the filter.

To compare the frequential filtering to the spatial one, we focus on the high-

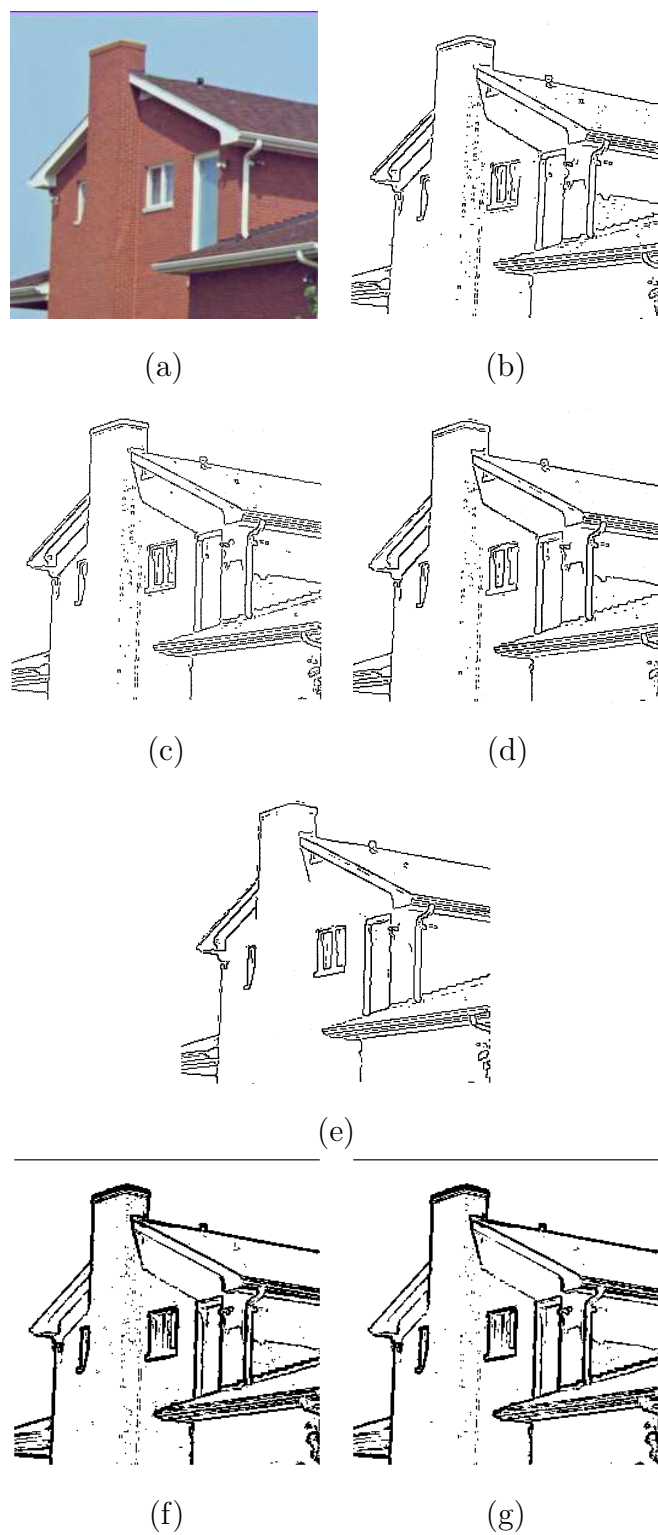


Fig. 11. **Different spatial gradients on the "house" image** : (a) "House" original image; (b) Marginal approach; (c) Di Zenzo approach; (d) First Carron approach; (e) Second Carron approach; (f) our method; (g) our method with logarithmic approach.

pass filtering

$$H(S, T) = 1 \text{ for } (|S| > a, |T| > b) \text{ and } 0 \text{ otherwise, with } a, b \in \mathbb{R}$$

Indeed we notice through the quaternionic spectrum study that there is a likeness of organisation as in the classical complex spectrum. As a consequence, high frequency selection will give weight to ruptures and thus contours.

Figure 12 shows that frequency filtering preserves the original colours and the high frequency content is really isolated from the rest of the image. In fact, the contours of the top and bottom boxes appear green and white in Figure 12g and the circle and quadrilateral are red and blue in Figure 12h as in the original image (Figure 12e). These remarks are also valid on the contours made on the Lenna image as we can see the details of her hat in Figure 12c and mouth in Figure 12d. We see that information on edges is vectorial as it appears in colours. A scaling process between 0 and 255 has been made after IDQFT using the min and max of each component. As the method uses the windowing concept to filter the image in the frequency domain, we can observe that there are some oscillations on edges detected in the high-pass filtered pictures. This windowing process in the quaternionic spectral domain leads to equivalent artefacts than those produced if it was done on a greyscale image spectrum : the Fourier transform of the rectangle function is the sinc (sine cardinal) function. However, even if this statement is not true anymore with the formalism of quaternions (from the anti-commutativity of the product), we observe that it still remains the same kind of border effects. Note that the colour artefacts are just the conjugate colours of the edges in the RGB colour domain as we see in Figure 12h where the red (resp. blue) colour of the circle (resp. quadrilateral) is oscillating with green (resp. yellow).

Figure 13 shows that this spectrum strategy is at least good enough to detect colour edges properly. A edge map is made by thresholding the absolute values of the filtered images. This method seems however more sensitive to small details than the one presented on the spatial filtering section but it may give more details than the spatial approach with not saturated colours. Indeed we can see in Figure 13c that the gutters and drainpipes of the roof are well detected by the frequential method. They are not detected by the spatial one because they are quite white (white has a zero saturation level). Furthermore, this approach can filter both in low-pass and high-pass bands and it can be generalized to band-pass by selecting the proper windowing scheme in the spectrum domain.

Notice that the experiments show only results with the  $\mu$  parameter of the DQFT and IDQFT equal to  $\mu_{grey}$ . Finally taking the interpretation of the quaternionic spectrum of the first section we may be able to make spectrum filters which can extract only one component or any combinaison of them.

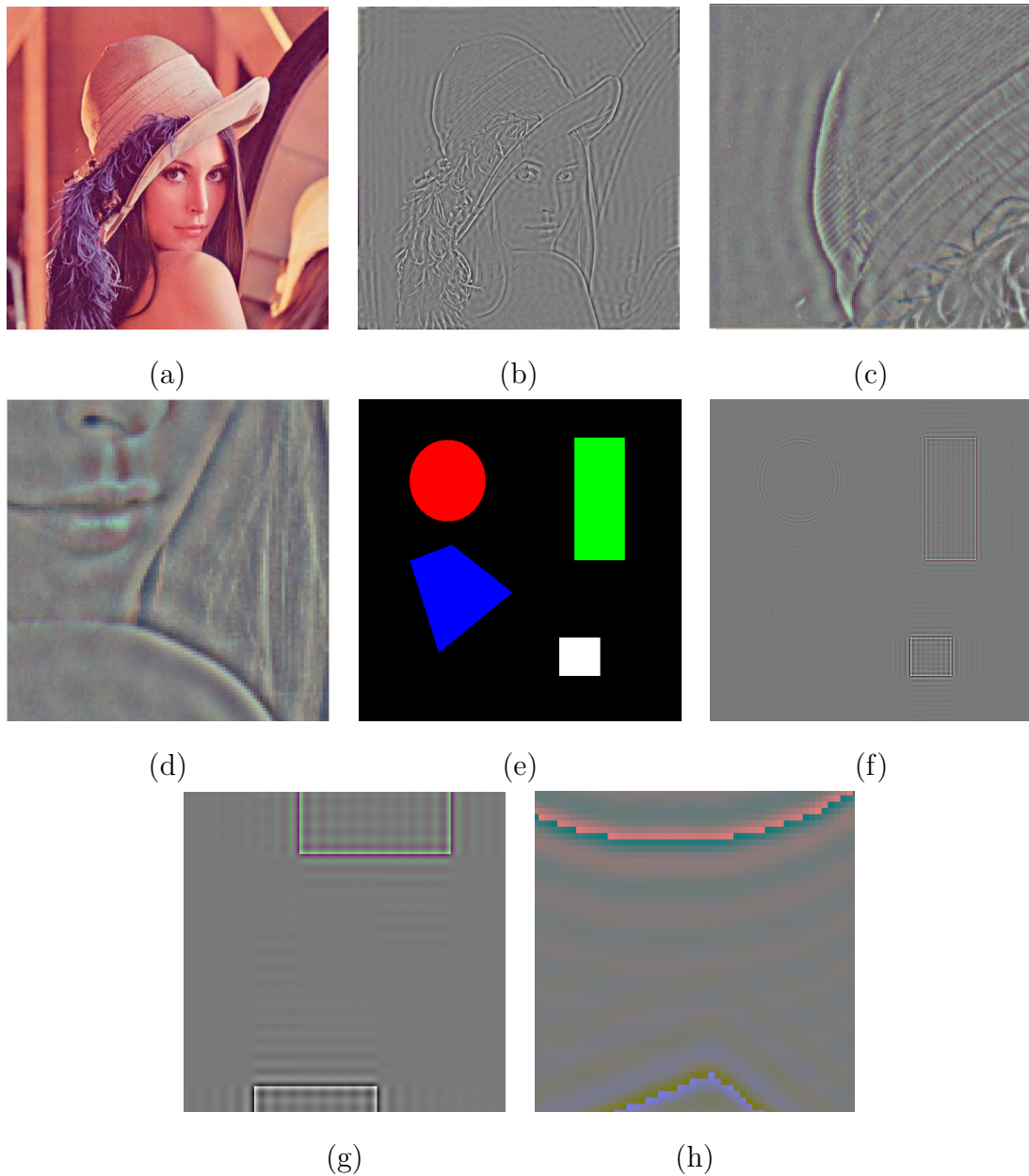


Fig. 12. **Quaternionic high-pass filtering results:** (a) Lenna original image; (b) highpass filter applied on (a); (c) details of the hat; (d) details of the face; (e) hand-made colour image; (f) high-pass filter applied on (e); (g) details of the green and white boxes edges; (h) details of the red circle and blue quadrilateral edges. Frequency filtering preserves the original colours.

Speaking about performances, it takes two classical complex fast Fourier transforms to perform a DQFT or IDQFT. To process both DQFT and IDQFT is so equivalent to a complexity in  $\mathcal{O}(N^2 \ln(N^2))$ . The windowing process is a product term by term between the spectrum and a 2D rectangle function. This process has a complexity in  $\mathcal{O}(N^2)$ . The all method uses the two previous algorithms leading the total complexity of the process in  $\mathcal{O}(N^2 + N^2 \ln(N^2)) =$

$\mathcal{O}(N^2 \ln(N^2))$ . This is a bit slower than the spatial method.

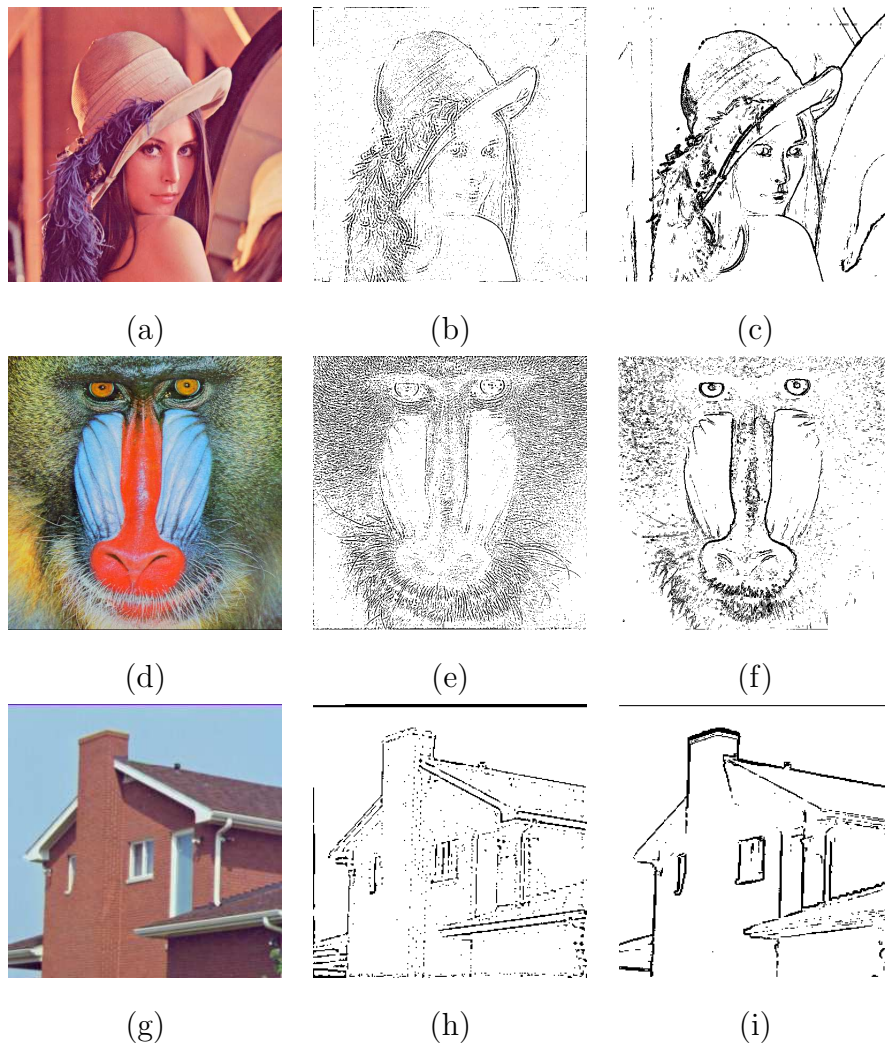


Fig. 13. **Comparison between high-pass and spatial filtering:** (a) Lenna original image; (b) highpass filtering's edge map; (c) spatial gradient's edge map; (d) mandrill original image; (e) highpass filtering's edge map; (f) spatial gradient's edge map; (g) house original image; (h) highpass filtering's edge map; (i) spatial gradient's edge map.

#### 4 Conclusion

In this paper, we analysed the properties of the quaternionic Fourier spectrum. This contributed first, to reconstruct after IDQFT and without any loss of information a quaternionic spatial colour image composed of three imaginary components only. Secondly, this gave us an interpretation of quaternionic Fourier coefficients influence on the spatial domain with both calculus and graphical illustrations. When initializing the real part of the spectrum with

a pair of constants respecting proper symmetries, the corresponding spatial domain presents odd oscillations dependent on the  $\mu$  parameter of the transformation. However, spectrum pairs of Dirac initialization made on imaginary component influences the spatial domain with even oscillations independently from the  $\mu$  parameter. As in the complex Fourier analysis, the quaternionic spectrum can be used to detect spatial orientations. Then in a second part, we applied the previous digital concepts to propose a new quaternionic colour vectorial gradient. This gave enthusiastic results as it takes advantages of both vectorial and perceptual approaches of spatial filtering for a RGB colour space approach. In addition, we used the interpretation of the spectrum to create frequency quaternionic filters that gave similar results than complex frequency filters on greyscale images. In that way, both spatial and spectrum approaches have been discussed to get a wider vision on filtering with quaternions. Perspectives are first to enhance the spatial vectorial filter in order to take the saturation reluctance into account, thus achieving higher efficiency by giving more power to intensity and hue values when needed. The frequential approach can as well be improved first by using a smoother function than the rectangle one to process the spectrum filtering and soften the border effects leading to colour artefacts. Secondly, we can select in the Fourier domain the wanted components as described by the spectrum interpretation of the first section. Finally, as quaternions do not seem to give information to compare colour components between themselves but more independent component analysis, geometric algebra which manipulates vectors but also multivectors may represent a useful tool to achieve new results.

## A Appendix

### A.1 Digital study of the colour spectrum

This section shows more details on how, an initialization made in the quaternionic spectrum, influences the spatial domain after IDQFT.

A problem relies on the fact that the spectrum must present the previous symmetry conditions (refer to section 2.2), and thus the pixel at coordinates  $(-S_0, -T_0)$  must be initialized with amplitude that respects the conditions. Eventually there are two points initialized in the spectrum in order to find a spatial image after IQFT without any loss of information. There are different cases for initialization, as reported in the following.

- *Initialization on the real component*

In this case, the initialization requires the  $Q_r(S_0, T_0) = K_r$  and  $Q_r(-S_0, -T_0) =$

$-K_r$  conditions. After IDQFT the spatial image is represented on its imaginary components as follows:

$$\begin{aligned} q_r(s, t) &= 0 \\ q_i(s, t) &= 2K_r\mu_i \sin\left(2\pi\left(\frac{S_0s}{N} + \frac{T_0t}{M}\right)\right) \\ q_j(s, t) &= 2K_r\mu_j \sin\left(2\pi\left(\frac{S_0s}{N} + \frac{T_0t}{M}\right)\right) \\ q_k(s, t) &= 2K_r\mu_k \sin\left(2\pi\left(\frac{S_0s}{N} + \frac{T_0t}{M}\right)\right) \end{aligned}$$

Initialize the real component of the spectrum leads, after IQFT process, to odd variations (for the sinus is an odd function). These variations are described by the imaginary component(s) used to set the analysing direction  $\mu = \mu_i i + \mu_j j + \mu_k k$ . As for a classical frequency representation, we observe that the frequency coordinates  $(S_0, T_0)$  are associated with the direction and the repetition density of the analyzed pattern.

- *Initialization on an imaginary component*

In this case the initialization requires  $Q_e(S_0, T_0) = Q_e(-S_0, -T_0) = K_e$  (with  $e = i, j$  or  $k$ ) conditions. After IDQFT the spatial image corresponding to e-imaginary component is represented on its following cartesian form

$$\begin{aligned} q_e(s, t) &= 2K_e \cos\left(2\pi\left(\frac{S_0s}{N} + \frac{T_0t}{M}\right)\right) \\ q_{e'}(s, t) &= 0 \text{ with } e' \neq e \end{aligned}$$

Initialize an (several) imaginary component(s) of the spectrum leads, after IQFT process, to even oscillations (for the cosinus is a even function) described on the same imaginary component(s). We observe that the analysing direction  $\mu$  chosen in the IDQFT has no influence.

## A.2 Quaternionic Graphical Spectrum Illustration

### A.2.1 Initialization on a spectrum's imaginary part with any $\mu \in \mathbb{S} \cap \mathbb{P}$

As we saw in the previous section, to set a pair of constants that follows the necessary conditions on one imaginary component of the quaternionic spectrum leads to a spatial oscillation on the same component after processing IDQFT (cf. Figure A.1). For example if the initialization is done on the first frequency component, the spatial oscillations that arise from IDQFT are on the first spatial component coding the image, that is to say the red channel if working in RGB colour space. The initialization can be done on several

components, in that case, the result affects the same components that have been modified. In our case as the following examples are taken from a RGB colour space, multiple initializations (always under the conditions for correct spatial reconstruction) on the spectrum produce spatial oscillations following the rules of the additive synthesis of colours. So if we initialize the spectrum on each imaginary component with the same couple of constants, the spatial result after IDQFT on a RGB colour space is grey oscillations. The  $\mu$  parameter does not interfere in this case.

### A.2.2 Initialization on the spectrum's real part with any $\mu \in \mathbb{S} \cap \mathbb{P}$ but $\mu \neq \mu_{Grey}$

It was shown in Section 2.3 that the initialization on the spectrum could be done on the real component. In that case, we can also get different kinds of oscillations after IDQFT was performed, thus showing that the conditions enunciated before are preserved. Oscillations after IQFT process are on the same imaginary components involved in the initialization of the pure unit quaternion direction  $\mu$ . In other words, working in RGB colour space implies that, to get red oscillations, the  $\mu$  parameter must be equal to  $i$  (cf. Figure A.2). Oscillations composed of numerous colours can be achieved in setting the  $\mu$  parameter properly, for instance  $\mu = \frac{i+j}{\sqrt{2}}$  leads to yellow variations in the RGB colour space after IDQFT.

### A.2.3 Geometric Variations

In the complex plane, coordinates of the spectrum coefficients involved in the quaternionic Fourier space's initialization are really important parameters. Indeed, the resulting oscillations by IDQFT process have a geometric orientation linked to this. Supposing that coordinates are given in  $\mathbb{Z}^2$  with the pixel  $O(0,0)$  in the image centre (whereas on the top-left corner as often), the initialization of the spectrum at coordinates  $(S_0, T_0)$  and  $(-S_0, -T_0)$  results, through IDQFT process, in a 2D oscillation (sinus and cosinus) following the axis made by this two pixels.

In Figure A.3, numerous geometric oscillations are shown by modifying the coordinates of the pixels pair implicated by the initialization but with the same way to set the spectrum components.

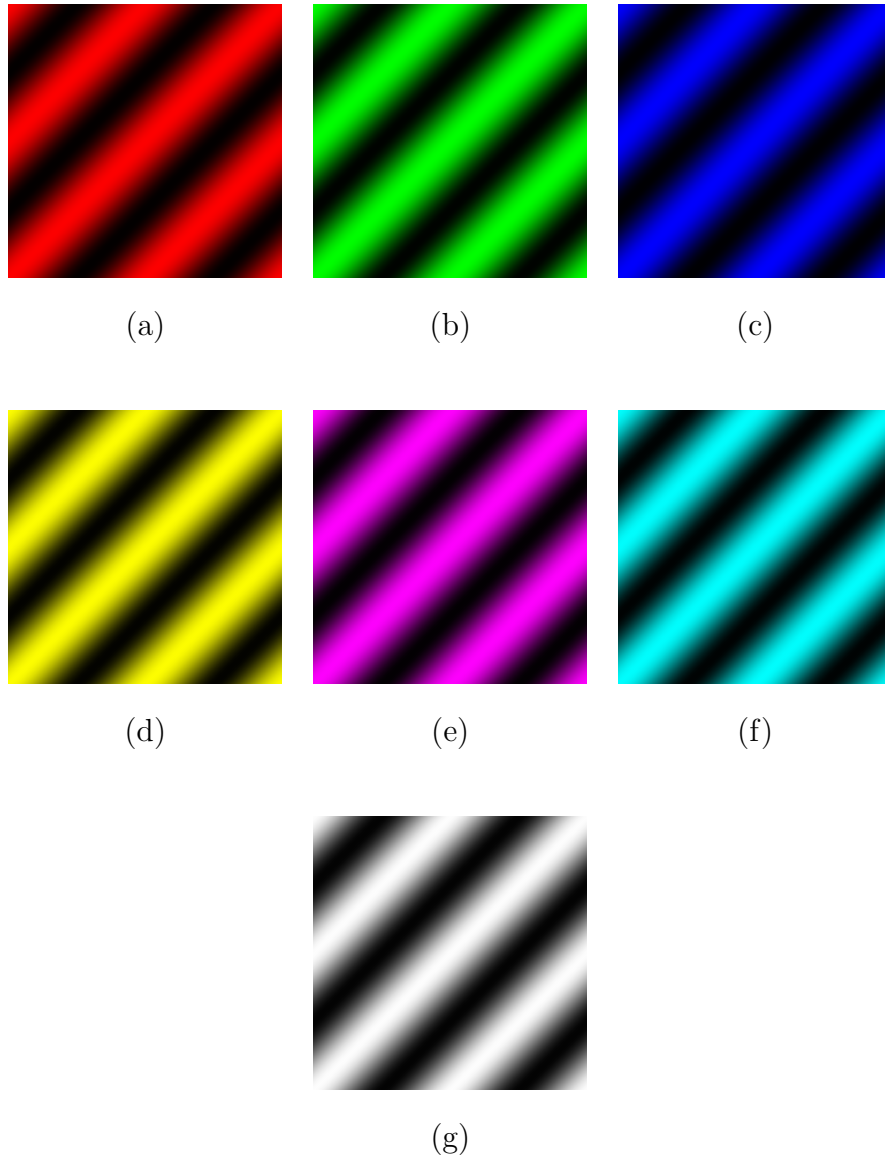


Fig. A.1. **Initialization examples with  $\mu = \mu_{Grey} = \frac{i+j+k}{\sqrt{3}}$ :** (a)  $Q_i(2,2) = Q_i(-2,-2) = K_i$ ; (b)  $Q_j(2,2) = Q_j(-2,-2) = K_j$ ; (c)  $Q_k(2,2) = Q_k(-2,-2) = K_k$ ; (d)  $Q_i(2,2) = Q_i(-2,-2) = K_i$  and  $Q_i(2,2) = Q_i(-2,-2) = K_i$ ; (e)  $Q_j(2,2) = Q_j(-2,-2) = K_j$  and  $Q_j(2,2) = Q_j(-2,-2) = K_j$ ; (f)  $Q_k(2,2)Q_k(-2,-2) = K_k$  and  $Q_k(2,2) = Q_k(-2,-2) = K_k$ ; (g)  $Q_i(2,2) = Q_i(-2,-2) = K_i$ ,  $Q_j(2,2) = Q_j(-2,-2) = K_j$  and  $Q_k(2,2) = Q_k(-2,-2) = K_k$ .

## B Acknowledgments

The author thanks Emeric Rollo[18] for his contribution to the spatial colour gradient part of this work. Thanks as well to Poitou-Charentes Region board and PIMHAI, INTERREG IIIB "Arc Atlantique" project, which have funded this work.

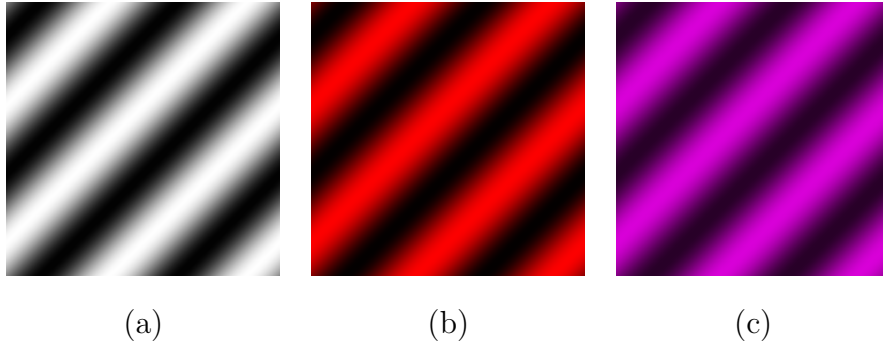


Fig. A.2. Initialization examples with  $\mu \neq \mu_{Grey}$  and  $Q_r(2,2) = -Q_r(-2,-2) = K_r$  (a)  $\mu_{Grey} = \frac{i+j+k}{\sqrt{3}}$ ; (b)  $\mu_{Red} = i$ ; (c)  $\mu_{Magenta} = \frac{i+k}{\sqrt{2}}$ .

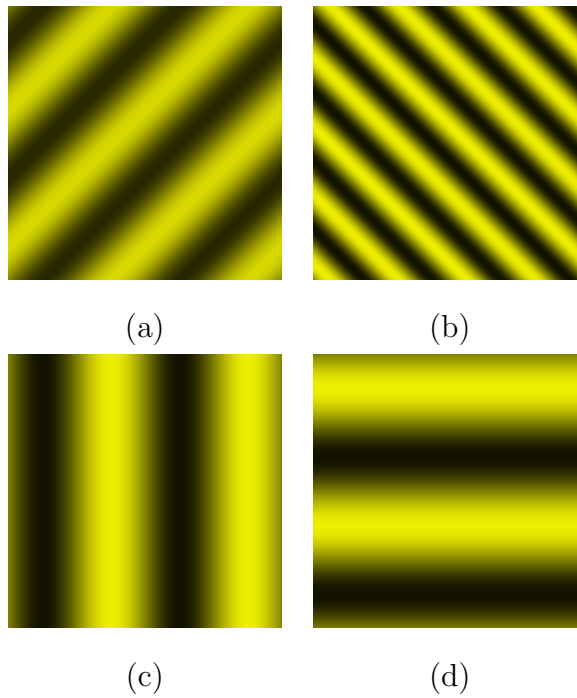


Fig. A.3. Geometric oscillation examples initialization with  $\mu_{Yellow} = \frac{i+j}{\sqrt{2}}$  (a)  $Q_r(2,2) = -Q_r(-2,-2) = K_r$ ; (b)  $Q_r(4,-4) = -Q_r(-4,4) = K_r$ ; (c)  $Q_r(0,2) = -Q_r(0,-2) = K_r$ ; (d)  $Q_r(2,0) = -Q_r(-2,0) = K_r$ .

## References

- [1] Thomas Bülow, *Hypercomplex Spectral Signal Representations for the processing and Analysis of Images*, p.22, PhD Thesis, August 1999
- [2] T. Carron, *Segmentation d'images couleur dans la base Teinte-Luminance-Saturation : approche numerique et symbolique*, These de doctorat, Universite de Savoie, decembre 1995

- [3] S. Di Zeno, *A note on the gradient of multi-image*, in *Computer Vision, Graphics, and Image Processing*, vol.33, pp116-125,1986.
- [4] T.A. Ell and S.J. Sangwine,*Decomposition of 2D hypercomplex Fourier transforms into pairs of Fourier transforms*,in *Proc. EUSIPCO*,2000,pp.151-154
- [5] M. Felsberg and G. Sommer,*Optimized fast algorithms for the quaternionic Fourier transform*,in *8th Int. Conference on Computer Analysis of Images and Patterns*, Ljubljana,1999,vol.1689,p209-216
- [6] C. Fernandez-Maloigne, M.-C. Larabi, B. Bringier B, and N. Richard., *Spatial-temporal characteristics of the visual brain and their effects on colour quality evaluation*, in *AIC International Conference*, Granada, Spain, 813 May 2005.
- [7] P.H. Gosselin, *Quaternions et Images Couleurs*, DEA study with SIC laboratory in 2002, p.25-27
- [8] W.R. Hamilton, *Elements of Quaternions*. London, U.K.: Longman, 1866
- [9] Kelly D.H.,*Spatiotemporal variation of chromatic and achromatic contrast thresholds*. J. Opt. Soc. Am. 73(6):742750, 1983.
- [10] R. Lukac, K.N. Plataniotis, A.N. Venetsanopoulos, R. Bieda, and B. Smolka, *Color edge detection techniques*, in *Signaltheorie und Signalverarbeitung, Akustik und Sprachakustik, Informationstechnik*, W.E.B. Universitt Verlag, Dresden, vol. 29, pp. 21-47, 2003.
- [11] R. Lukac, B. Smolka, K. Martin, K.N. Plataniotis, and A.N. Venetsanopoulos, *Vector filtering for color imaging*, in *IEEE Signal Processing Magazine*, vol. 22, no. 1, pp. 74-86, January 2005.
- [12] R. Lukac and K.N. Plataniotis, *A taxonomy of color image filtering and enhancement solutions*, in *Advances in Imaging and Electron Physics*, (eds.) P.W. Hawkes, Elsevier, vol. 140, 2006, 187-264.
- [13] C.E. Moxey, S.J. Sangwine and T.A. Ell, *Vector Correlation of colour Images in First European Conference on Colour in Graphics, Imaging and Vision (CGIV 2002)*, University of Poitiers, France, 2-5 April 2002, The society for Image Science and Technology, pages 343-347.
- [14] C.E. Moxey, S.J. Sangwine and T.A. Ell, *Hypercomplex Correlation Techniques for Vector Images* in *IEEE Transactions on Signal Processing*, vol.51, July 2003, pages 1941-1953
- [15] Soo-Chang Pei, Jian-Jiun Ding and Ja-Han Chang,*Efficient Implementation of Quaternion Fourier Transform, Convolution, and Correlation by 2-D Complex FFT*, IEEE Trans. Signal Processing, vol.49, p2783-2797, Nov 2001
- [16] K.N. Plataniotis and A.N. Venetsanopoulos, *Color Image Processing and Applications*, Springer Verlag, 2000.
- [17] A.B. Poirson and B.A. Wandell. *Pattern-color separable pathways predict sensitivity to simple colored patterns*. in *Vision research*, march 1996.

- [18] E. Rollo, N. Richard, C. Fernandez Maloigne, *A perceptual colour image watershed*, SIC laboratory, internal report, may 2006
- [19] Sangwine, S.J., *Colour image edge detector based on quaternion convolution*, in *Electronics Letters*, 34, (10), May 14 1998, 969-971.
- [20] Sangwine, S.J., *Colour in Image Processing*, in *Electronics and Communication Engineering Journal*, 12, (5), October 2000, 211-219.
- [21] S.J. Sangwine and T. Ell, *Hypercomplex Fourier transforms of colour images*. In *Proc. ICIP*, volume 1, pages 137-140, Thessaloniki, Greece, 2001
- [22] S.J. Sangwine and T.A. Ell, *Mathematical Approaches to Linear Vector Filtering of colour Images* in *First European Conference on Colour in Graphics, Imaging and Vision (CGIV 2002)*, University of Poitiers.
- [23] Wandell, *Color appearance : the effects of illumination and spatial patterns*, Nat. Acad. Sci. USA 90, pp.9778-9784, 1993.